Quantitative CT Analysis in Chronic Hypersensitivity Pneumonitis: A Convolutional Neural Network Approach

Article *in* Academic Radiology · November 2020

DOI: 10.1016/j.acra.2020.10.009

CITATIONS
3

READS
83

9 authors, including:

Lorenzo Aliboni
Radiomics
12 PUBLICATIONS **19** CITATIONS
SEE PROFILE

Olívia Meira Dias
Hospital Israelita Albert Einstein
67 PUBLICATIONS **287** CITATIONS
SEE PROFILE

Francesca Pennati
Politecnico di Milano
69 PUBLICATIONS **229** CITATIONS
SEE PROFILE

Bruno Guedes Baldi
University of São Paulo
149 PUBLICATIONS **820** CITATIONS
SEE PROFILE

Original Investigation

Quantitative CT Analysis in Chronic Hypersensitivity Pneumonitis: A Convolutional Neural Network Approach

Lorenzo Aliboni, MSc*, Olívia Meira Dias, PhD, MD*, Francesca Pennati, PhD, Bruno Guedes Baldi, PhD, MD, Marcio Valente Yamada Sawamura, MD, Rodrigo Caruso Chate, MD, Carlos Roberto Ribeiro Carvalho, PhD, MD, André Luis Pereira de Albuquerque, PhD, MD, Andrea Aliverti, PhD

Rationale and Objectives: Chronic hypersensitivity pneumonitis (cHP) is a heterogeneous condition, where both small airway involvement and fibrosis may simultaneously occur. Computer-aided analysis of CT lung imaging is increasingly used to improve tissue characterization in interstitial lung diseases (ILD), quantifying disease extension, and progression. We aimed to quantify via a convolutional neural network (CNN) method the extent of different pathological classes in cHP, and to determine their correlation to pulmonary function tests (PFTs) and mosaic attenuation pattern.

Materials and Methods: The extension of six textural features, including consolidation (C), ground glass opacity (GGO), fibrosis (F), low attenuation areas (LAA), reticulation (R) and healthy regions (H), was quantified in 27 cHP patients (age: 56 $\pm$ 11.5 years, forced vital capacity [FVC]% = 57 $\pm$ 17) acquired at full-inspiration via HRCT. Each class extent was correlated to PFTs and to mosaic attenuation pattern.

Results: H showed a positive correlation with FVC%, FEV1% (forced expiratory volume), total lung capacity%, and diffusion of carbon monoxide (DLCO)% (r = 0.74, r = 0.78, r = 0.73, and r = 0.60, respectively, $p < 0.001$). GGO, R and C negatively correlated with FVC% and FEV1% with the highest correlations found for R (r = −0.44, and r = −0.46 respectively, $p < 0.05$); F negatively correlated with DLCO% (r = −0.42, $p < 0.05$). Patients with mosaic attenuation pattern had significantly more H ($p = 0.04$) and lower R ($p = 0.02$) and C ($p = 0.0009$) areas, and more preserved lung function indices (higher FVC%; $p = 0.04$ and DLCO%; $p = 0.05$), but did not show more air trapping in lung function tests.

Conclusion: CNN quantification of pathological tissue extent in cHP improves its characterization and shows correlation with PFTs. LAA can be overestimated by visual, qualitative CT assessment and mosaic attenuation pattern areas in cHP represents patchy ILD rather than small-airways disease.

Key Words: Convolutional neural network; Quantitative CT imaging; Chronic hypersensitivity pneumonitis.

Abbreviation: consolidation C, **chronic hypersensitivity pneumonitis** cHP, **ground glass opacities** GGO, **interstitial lung disease** ILD, **fibrosis** F, **hypersensitivity pneumonitis** HP, **low attenuation areas** LAA, **mosaic** M, **healthy** H, **non-mosaic** NM, **reticulation** R

INTRODUCTION

Hypersensitivity pneumonitis (HP) is a fibrotic lung disease with variable clinical symptoms, caused by the inhalation of specific organic antigens or low molecular weight substances in genetically susceptible individuals (1−3). Chronic-HP (cHP) represents its final stage, in which prolonged antigenic exposure causes fibrosis. Recent published guidelines have emphasized the presence of radiographic or histopathological fibrosis as the primary determinant of prognosis in HP, and a new disease categorization into "fibrotic" and "non fibrotic HP" instead of "acute, " "subacute," and "chronic HP. " Although our study cohort is

Acad Radiol 2020; ■:1–10

From the Dipartimento di Elettronica, Informazione e Bioingegneria, Politecnico di Milano, Milan, Italy (L.A., F.P., A.A.); Pulmonary Division, Instituto do Coracao (InCor), Hospital das Clinicas HCFMUSP, Faculdade de Medicina, Universidade de Sao Paulo, Sao Paulo, SP, Brazil (O.M.D., B.G.B., C.R.R.C., A.L.P.d.A.); Radiology Division, Instituto do Coracao (InCor), Hospital das Clinicas HCFMUSP, Faculdade de Medicina, Universidade de Sao Paulo, Sao Paulo, SP, Brazil (M.V.Y.S., R.C.C.). Received August 2, 2020; revised October 1, 2020; accepted October 4, 2020. **Address correspondence to:** L.A. e-mail: lorenzo.aliboni@polimi.it

* LA and OMD equally contributed to this manuscript.

https://doi.org/10.1016/j.acra.2020.10.009

comprised of patients with the now called "fibrotic" HP, we will still adopt the term cHP since the study was conducted before the publication of these guidelines.

Although cHP may be radiologically heterogeneous, high-resolution computed tomography (HRCT) has a pivotal role in differentiating cHP from other interstitial lung diseases (ILD). In advanced stages, cHP is characterized by CT findings of centrilobular ground glass opacities and fibrosis, with reticulation and traction bronchiolectasis causing architectural distortion with or without honeycombing, generally with a predominance of upper and middle lung zones (4). Mosaic attenuation pattern, defined as a patchwork of lobular regions of differing attenuation (5), can be frequently found in cHP and has been previously described as a sign suggestive of small airway involvement and eventually, air trapping (6,7). However, mosaic attenuation pattern may also be produced by ground glass interstitial or airspace infiltration, in which areas of higher attenuation representing the interstitial process may be juxtaposed to areas of lower attenuation representing normal lung (3). Visually HRCT interpretation is challenging and relies on radiologist's expertise, is time consuming and lacks objectivity and quantification.

Computer-aided analysis of HRCT has been reported for detecting and classifying different lung abnormalities in ILD and for quantifying disease extension and progression.

One possible approach is to extract relevant textural features from regions of interest and use machine learning techniques to classify each lung region into healthy and pathological textural classes. Texture analysis in ILD focused on finding optimal textural features, including first and second order statistical features extracted from grey-level distributions, fractal dimension (8,9), wavelet transform (10,11) and filtering techniques (12).

Deep learning approaches based on convolutional neural networks (CNN) have been explored in the last few years. CNNs learn features and train a classifier at the same time, by minimizing the classification error. Networks trained from scratch (13) or pretrained networks appropriately fine-tuned for the ILD pattern detection and classification (14,15) have shown high performances.

We hypothesized that quantitative CT analysis may improve characterization of cHP. The aims of this study were: (1) to develop a CNN method to quantify the extent of the different pathological imaging classes in cHP; (2) to determine the correlation between each class and pulmonary function tests (PFTs) on an independent cohort of cHP patients, and (3) to quantitatively characterize mosaic attenuation pattern in cHP.

MATERIALS AND METHODS

Study Subjects

This study is part of a comprehensive study evaluating small airway involvement in cHP patients (ClinicalTrials.gov Identifier NCT 02523833) with volumetric CT scans, PFTs, forced oscillation technique examinations, and cardiopulmonary exercise testing. From September 2015 to March 2017, 177 patients with confirmed cHP diagnoses, seen at the ILD outpatient clinic of the Pulmonary Division of the Hospital das Clinicas of the University of São Paulo, were prospectively evaluated and 27 were enrolled (Fig 1). The exclusion criteria considered factors related to disease severity, which would preclude patients to perform cardiopulmonary exercise testing as part of our study protocol. cHP diagnosis was based on CT findings (fibrotic involvement of the pulmonary parenchyma), known antigenic exposure, exclusion of other possible diagnoses and compatible histology upon transbronchial or open lung biopsy, or bronchoalveolar lavage with lymphocytosis above 30%. In patients without fibrosis on CT scans, histological evidence of fibrosis was considered for inclusion. The study protocol was approved by the local research ethics committee (SDC 3966/13/091), and all patients signed informed consent.

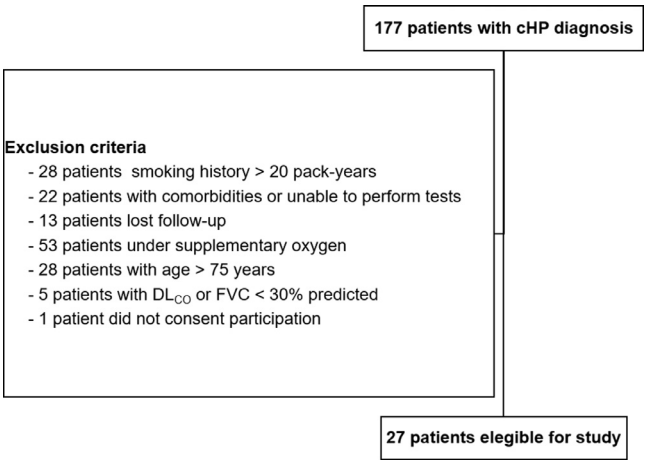

Figure 1. Study recruitment protocol. cHP, chronic hypersensitivity pneumonitis; DLCO, pulmonary diffusion of carbon monoxide; FVC, forced vital capacity.

CT scanning protocol

Patients underwent CT scanning on a Brilliance 16P scanner (Philips Medical Systems, Andover, MA) at suspended full-inspiration after standardized breathing instructions, using a weight-based CT technique for dose minimization (16). Imaging parameters were tube voltage, 120−140 kVp; tube current, 30 mAs; matrix, 512 × 512; slice thickness, 1.0 mm; reconstruction kernel, B filter.

Pulmonary function tests

PFTs were performed following ERS/ATS guidelines (17−19). Spirometry was performed using a calibrated pneumotachograph (Medical Graphics Corporation, St. Paul, MN). Lung volumes and diffusion of carbon monoxide (DLCO) were measured with a body plethysmograph (Elite Dx, Elite Series; Medical Graphics Corporation). Forced vital

capacity (FVC), forced expiratory volume in 1 second (FEV_1), total lung capacity (TLC), residual volume (RV), and DLCO were obtained. Values were expressed as a percentage of predicted values according to the prediction equations derived from the Brazilian population (20,21).

CNN design

Data

The dataset used for training and testing the proposed network was composed of the publicly available multimedia database of ILDs from the University Hospital of Geneva (22), which consists of 109 HRCT scans of different ILD patients. In this dataset, manual annotations for 17 different lung patterns based on definitions from the glossary of terms for Thoracic imaging from the Fleischner Society (5) are also provided, along with clinical parameters from patients with histologically proven diagnoses of ILDs. Manual annotations do not contain ambiguous regions presenting more than one pattern. We evaluated five pathological patterns according to their relevance in cHP and to the samples' availability: consolidation (C), fibrosis (F), reticulation (R), ground glass opacity (GGO), and low attenuation areas (LAA), a category defined by the sum of emphysema and air trapping areas. Healthy (H) tissue was also added for a total of six classes.

ROIs preprocessing

ROIs were preprocessed by clipping intensity values between −1000 and 200 HU and mapping them in the range [0, 1] (13,23). To standardize ROIs shape and size, we extracted nonoverlapping squared patches sized 32 × 32. ROIs were accepted only if at least 80% of the area was included in the original annotations (22). ROIs numerosity and distribution among the classes and datasets is reported in Table 1. For each class, 100 patches were randomly selected for the test and 100 for the validation set.

ROIs extraction and preprocessing were performed in Python.

CNN Architecture

The network architecture (Fig 2) is based on the considerations in Anthimopoulos et al. (13). We adopted a shallower network with fewer layers to cope with reduced computational power. The input images are convolved by three 2D convolutional layers with minimal kernel size (2 × 2) and number of kernels of each layer equal to 16, 32, 64,

TABLE 1. Number of Extracted Regions Per Class and Dataset Composition

	Class					
	C	F	GGO	H	LAA	RET
Train set	161	889	588	926	253	204
Validation set	100	100	100	100	100	100
Test set	100	100	100	100	100	100
Total	361	1089	788	1126	453	404

Abbreviations: C, consolidation; F, fibrosis; GGO, ground glass opacities; H, healthy; LAA, low attenuation areas; R, reticulation; ROIs, regions of interests.

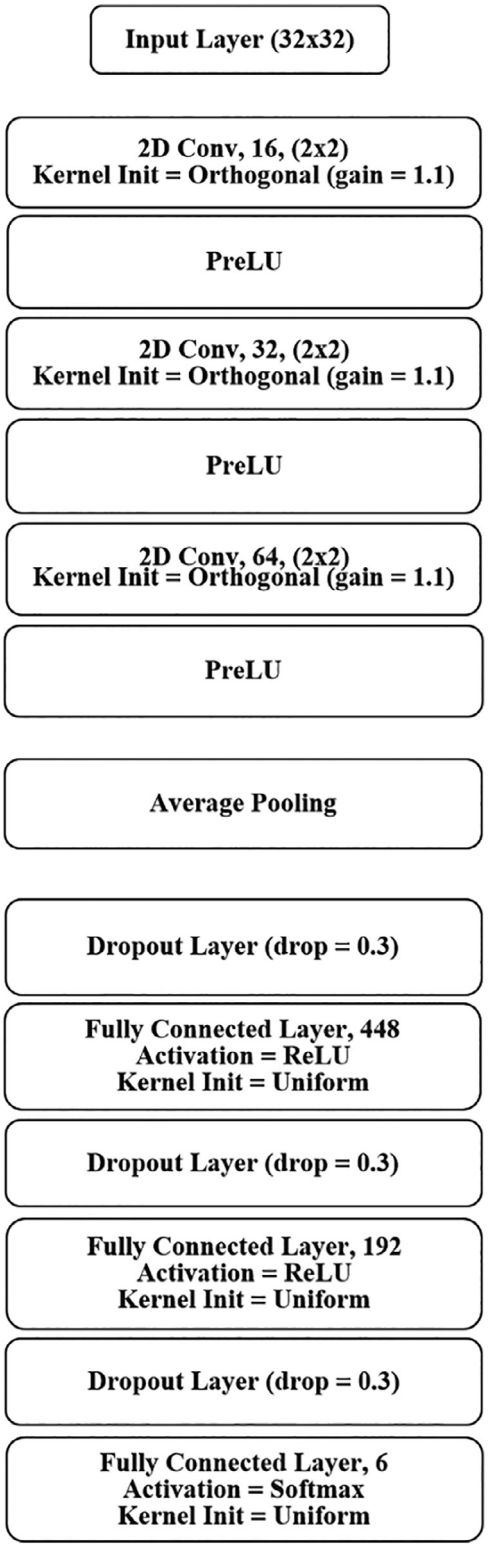

Figure 2. Architecture of the proposed CNN. PReLU, parametric linear rectified unit; ReLU, rectified linear unit.

respectively. Orthogonal initialization (with a scaling parameter equal to 1.1) was used for the kernels of all convolution layers. A parametric linear rectified unit (PReLU), was used as activation function of the convolutional layers. One single average pooling layer is added before the fully connected layers. A dropout layer (dropout rate = 0.3) is introduced before each dense layer. A total of three dense layers was used (uniform initialization), the number of nodes was chosen equal to 448, 192 and 6 for the first, second, and third layer, respectively. A linear rectified unit (ReLU) activation function was chosen for the first and second dense layer, while a softmax activation was adopted for the last one.

Training and Performance Evaluation

We adopted an Adam optimizer (24) to minimize a class-weighted categorical cross-entropy. The choice of a weighted minimization partially addresses the unbalance in our training dataset (25). Optimizer learning rate was set to 0.001, the exponential decay rates for the moving averages of the gradient = 0.9 and squared gradient = 0.999. Batch size was set to 64. Training procedure stopped when the validation loss did not improve for more than 200 epochs.

Data augmentation was performed on the training data by three label preserving transformations: horizontal flipping, vertical flipping and random rotation in the range [0, 60°].

CNN performances on the test dataset were assessed by calculating accuracy and F1 score average (F1 $score_{avg}$):

$$Accuracy = \frac{TP + TN}{TP + TN + FP + FN}$$

$$F1\ score_{avg} = \frac{1}{3} \times \sum_{class=1}^{6} \frac{precision_{class} \times sensitivity_{class}}{precision_{class} + sensitivity_{class}}$$

where

$$Precision_{class} = \frac{TP_{class}}{TP_{class} + FP_{class}}$$

$$Sensitivity_{class} = \frac{TP_{class}}{TP_{class} + FN_{class}}$$

and TP = true positives, TN = true negatives, FP = false positives, FN = false negatives.

Network development, training, and testing was performed using of Keras application user interface (26) ran on the top of TensorFlow library (27).

CNN Application to the full CT lung volume

The trained and tested CNN was applied to the full CT lung volume of the completely independent cohort of 27 cHP subjects to quantify the extent of each class. The lungs were automatically segmented from the CT images to separate lung parenchyma from the surrounding soft tissues. Segmentation algorithm (28) included: (1) wavelet preprocessing to make the segmentation more reliable to the anterior and posterior junctions; (2) selection of the optimal threshold to separate low density tissue from the surrounding chest wall (29); (3) subtraction of the airways reconstructed with a 3D confidence connected region growing and of the air surrounding the patient. Pulmonary vessels were isolated via a hessian-based filter (30) Lung and vessels segmentation was performed using the Insight toolkit library (ITK) of the National Library of Medicine (31).

The segmented volume was preprocessed by clipping in range [−1000, 200] HU and remapping to [0,1], to uniform it with the training data.

Network classification on the volume was performed slice-by-slice. A 32 × 32 squared window was placed on left corner of the image and progressively translated on the image with no overlapping. The network classified only regions containing background or vessels below 10% of the area. The extent of each class was expressed in percentage to total lung volume.

Mosaic attenuation analysis

Each patient was independently classified for mosaic attenuation by counting the number of secondary lobules with decreased attenuation on inspiratory images (32) by a pneumologist (O.M.D.) and a thoracic radiologist (R.C.C., with 16 years-experience) without knowledge of clinical information or histologic diagnosis.

- class 0 (no low attenuation lobules);
- class 1 (up to four lobules);
- class 2 (five or more lobules and involving two to four lobes);
- class 3 (five or more lobules in more than four lobes, the lingula being considered a separate lobe).

To avoid confounding with lobular areas normally found in normal subjects, scoring was limited to nondependent lung and away from the superior segment of the lower lobe, the tip of the lingula, the right middle lobe and within areas of severe fibrosis (32) Disagreements between classifications were resolved by consensus.

Patients were classified as "nonmosaic" (class 0 and 1, "NM") and "mosaic" (class 2 and 3, "M") and the extent of each lung imaging class was evaluated in both groups.

STATISTICAL ANALYSIS

Data are reported as mean ± standard deviation if normally distributed, or alternatively as median (25th−75th percentile).

The total percentage of each class quantified by the CNN was correlated to PFTs using a Spearman Correlation coefficient (r) on ranks.

To compare the pattern distribution and the PFTs in mosaic and nonmosaic patients, a *t* test or a Mann-Whitney test was applied for normal and not normal distributions, respectively.

Significance was set at $p < 0.05$.

Statistics was performed using SPSS version 25.0 (IBM Corp. Released 2017. IBM SPSS Statistics for Windows, Version 25.0.0.1 Armonk, NY).

RESULTS

Baseline characteristics of patients

Twenty-seven patients (59.3% females, age: 56 ± 11.5 years) were enrolled (Table 2). The main clinical symptoms were dyspnoea (85%) and cough (81%). Exposure to moulds (78%) and bird antigens (63%) were the most common etiologic agents. All patients had restrictive lung disease, with a mean FVC of 57 ± 17%, mean TLC of 65 ± 17% and median DLCO of 41 (31−62)%. Eighteen (67%) patients were under treatment and nine (33%) had previously received immunosuppression, mainly azathioprine and corticosteroids.

CNN evaluation

The training history for the network is reported in Figure 3a. During the training, accuracy on validation set increases and loss on the validation and training dataset similarly decreases, indicating no overfitting (i.e., trained model does not generalize to unseen cases, but fits well the training data). Figure 3b reports the results of the classification on the test set.

On the test set, an overall accuracy = 0.8550 and a F1 $score_{avg} = 0.8540$ were achieved. The individual F1 scores were the following: F1 $score_C = 0.8995$, F1 $score_F = 0.8295$, F1 $score_{GGO} = 0.8134$, F1 $score_H = 0.8764$, F1 $score_{LAA} = 0.9146$, F1 $score_R = 0.7904$. The stop condition was met after 562 epochs. Best accuracy was obtained for H and LAA patterns while the most misclassified pattern was R either to GGO or F.

Lung volume analysis and correlation to PFTs

Overall, H and GGO were the prevalent classes (respectively 24 ± 11% and 63 ± 11%), with high occurrence of R (8 [3−17]%) and negligible LAA (0.2 [0.05−1]%), F (0.8 [0.3−1]%) and C (0.5[0.07−0.9]%).

Table 3 shows high correlation between H and PFTs (FVC, r = 0.74, $p < 0.001$; FEV1, r = 0.78, $p < 0.001$, TLC, r = 0.73, $p < 0.001$ and DLCO, r = 0.604, $p < 0.001$). GGO, C and R negatively correlated with FVC and FEV1 with the highest correlation between R and FEV1 (r = −0.46, $p = 0.02$) and FVC (r = −0.44, $p = 0.02$). LAA showed no correlation with PFTs.

Figure 4 reports CNN maps in two representative patients. In patient 1 (FEV1 = 110%, FVC = 100%) H was the prevalent pattern (green, 59%), with limited manifestation of GGO (yellow, 18%). Patient 2 had lower PFTs (FVC = 39%, FEV1 = 33%) showing extensive GGO (yellow, 81%), moderate R (fuchsia, 21%) and a low extent of H (green, 5%).

TABLE 2. Baseline Characteristics of Patients with Chronic Hypersensitivity Pneumonitis

Patients n	27
Females n (%)	16 (59.3)
Age (years)	56 ± 11.5
Baseline dyspnea index (mMRC)	1 (1−2)
Smokers, n (%)	7 (26%)
Oxygen saturation at rest, %	94 ± 2
Symptoms at diagnosis	
Dyspnoea, n (%)	23 (85%)
Cough, n (%)	22 (81%)
Wheezing, n (%)	19 (70%)
Fever, n (%)	12 (44%)
Weight loss, n (%)	10 (37%)
Duration of symptoms, in months, median (range)	24 (12−36)
Pulmonary function testing	
FVC% predicted	57 ± 17
FEV1 % predicted	62 ± 16
FEV1 / FVC	0.87 ± 0.05
FEF25-75% predicted	100 ± 30
TLC % predicted	65 ± 17
RV % predicted	79 ± 24
RV/TLC % predicted	143 ± 38
DL_{CO} % predicted	41 (31−62)
Exposure	
Mould, n (%)	21 (78%)
Birds, n (%)	17 (63%)
Feather pillow, n (%)	6 (22%)
Others, n (%)	3 (11%)
No recognized exposure, n (%)	0 (0%)
Actual exposure / Previous exposure	4/23
Bronchoalveolar lavage, n (%)	20 (74%)
Lymphocytes count (median %)	22 (10−40)
CD4/CD8 ratio	0.46 (0.34−1.27)
Lung biopsy, n (%)	21 (78%)
Transbronchial, n (%)	16 (59%)
Surgical, n (%)	5 (19%)
Treatment	
Treatment, active/previous	18/9
Corticosteroids, n (%)	25 (93%)
Cytotoxic drugs, n (%)	13 (48%)

Data are reported as mean ± standard deviation if normally distributed, or alternatively as median (25th-75th percentile), and percentage.

Abbreviations: DLCO, diffusing capacity for carbon monoxide; FEV1, forced expiratory volume in 1 second; FEF, forced expiratory flow at 25%−75%; FVC = forced expiratory capacity; MRC, modified Medical research council; RV, residual volume; TLC, total lung capacity.

Mosaic attenuation analysis

10 patients had mosaic attenuation (M) and 17 patients did not (NM), with an inter-observer agreement of mosaic attenuation classification, based on visual analysis, of 67% - cases without agreement were solved by consensus.

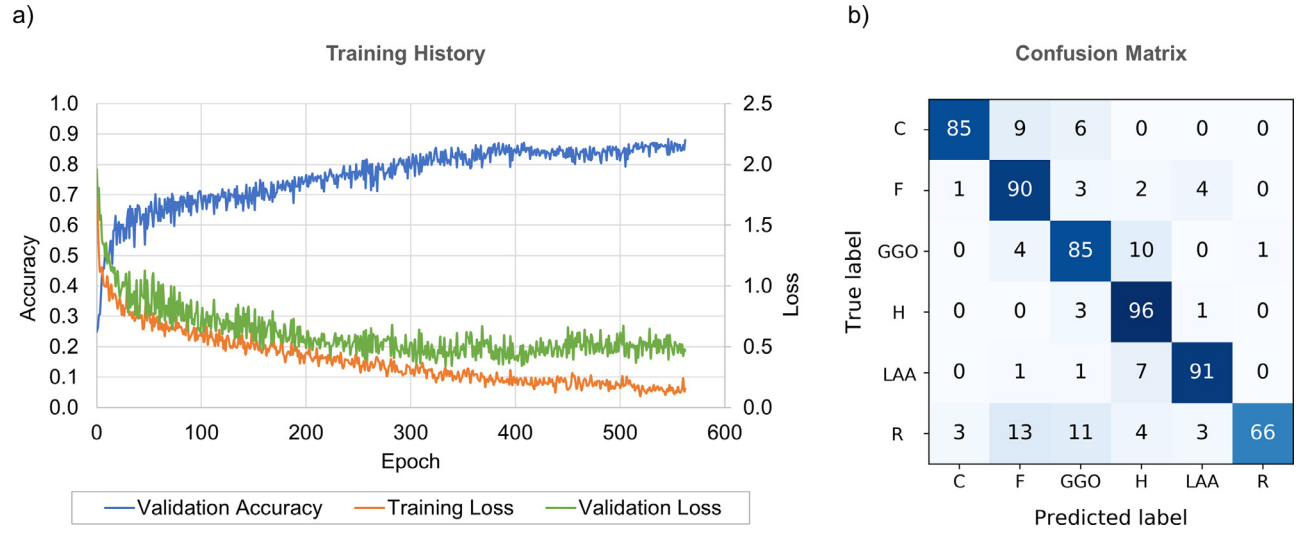

Figure 3. (a). Training history for the proposed model. In blue, the accuracy over the course of training increases over time up to 0.86 after 562 epochs. The green and yellow lines represent, respectively the loss (i.e., the fit between prediction and truth) on the validation and training datasets, which similarly decrease over time, indicating no appreciable overfitting. (b) Confusion matrixes obtained from the CNN classification on the test set.

Table 4 reports the quantitative CT analysis and PFTs in the two groups. On CT, patients with mosaic attenuation had lower C ($p = 0.009$) and R ($p = 0.02$) and higher H ($p = 0.04$). On PFTs, mosaic patients had higher FVC ($p = 0.04$) and DLCO ($p = 0.05$). Mosaic pattern did not show more correlation with pulmonary functional indices of air trapping.

DISCUSSION

CT analysis based on a CNN was performed in a group of cHP patients to objectively quantify the extent of healthy and pathological cHP patterns, showing correlation with PTFs, with the only exception being LAA. Also, patients with mosaic attenuation pattern have less fibrosis, consolidation and reticulation and significantly more preserved lung function than those without this pattern.

We proposed a CNN implemented and trained from scratch on publicly available dataset of ILD cases, which showed high accuracy in cHP patterns' detection. We adopted a shallow network due to the low-level characteristics we were analysing and to prevent overfitting. We kept the overall receptive field of the CNN small in order to keep low-level features which characterize the textural patterns under analysis and we avoided the use of pooling between the convolutional layers to prevent information loss (13). The introduction of

TABLE 3. Correlation Coefficients (r) Between the Extent of Lung Subcategories and Lung Function Parameters in Inspiration Scans

	Class Extent					
	C	F	GGO	H	LAA	R
TLC (%)	−0.364	−0.319	**−0.455***	**0.728****	0.014	−0.349
RV (%)	−0.154	−0.209	−0.271	0.274	−0.074	−0.024
RV/TLC ratio	0.242	0.276	−0.0769	−0.138	0.056	0.244
RV/TLC (%)	0.168	−0.001	0.00916	−0.194	−0.127	0.328
FVC (%)	**−0.427***	−0.355	**−0.391***	**0.743****	−0.004	**−0.439***
FEV1 (%)	**−0.420***	−0.342	**−0.401***	**0.782****	0.055	**−0.457***
FEV1/FVC (%)	0.103	0.238	0.133	0.0357	0.326	0.055
FEF25−75 (%)	−0.139	0.0122	−0.0486	0.355	0.275	−0.126
DLCO (%)	−0.326	**−0.418***	−0.318	**0.604****	−0.050	−0.274

Abbreviations: C, consolidation; DLCO, diffusion of carbon monoxide; F, fibrosis; FEF, forced expiratory flow between 25% and 75%; FEV1, forced expiratory volume 1 second; FVC, forced vital capacity; GGO, ground glass opacities; H, healthy; LAA, low attenuation areas; R, reticulation; RV, residual volume; TLC, total lung capacity.

Statistically significant relations are highlighted in bold.

* $p < 0.05$.

** $p < 0.001$.

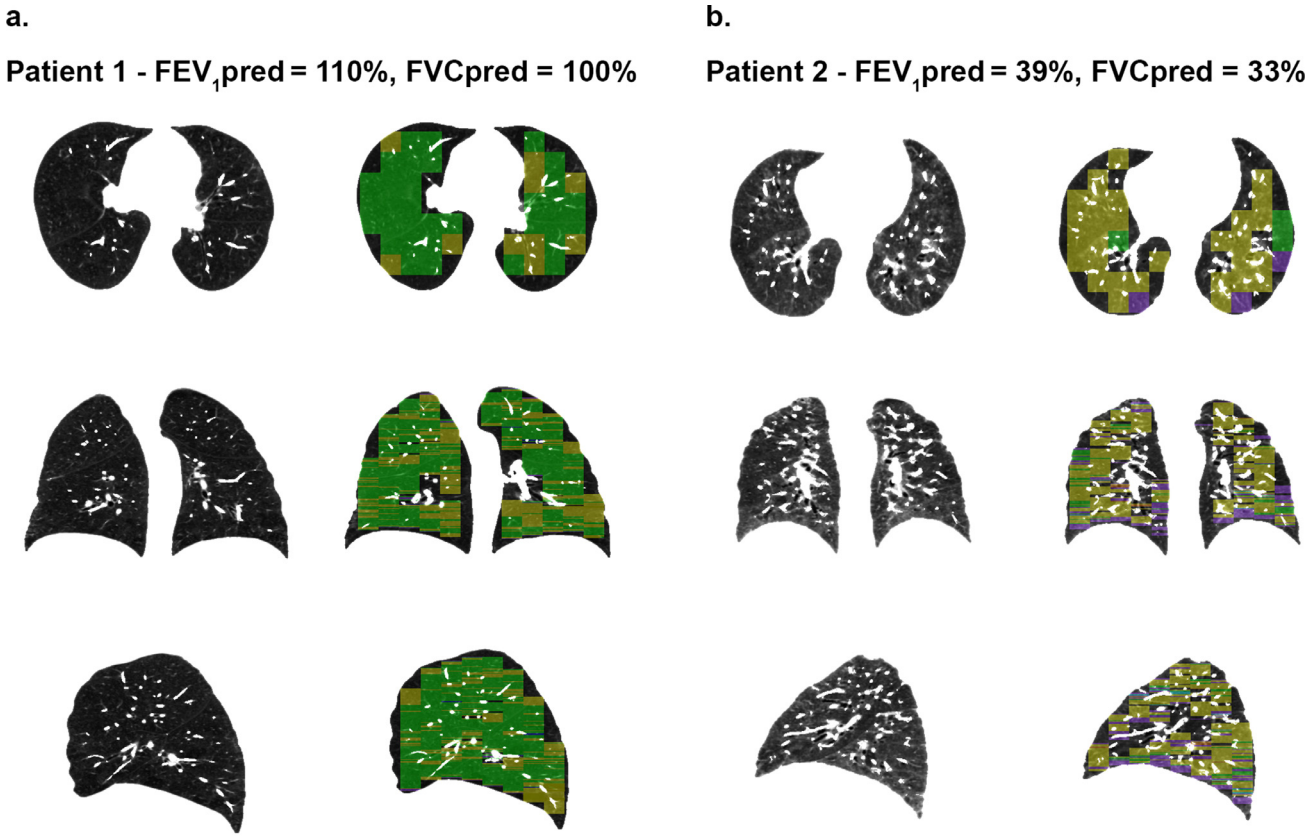

Figure 4. Exemplative CNN classification of cHP patterns on a CT scan from two representative patients. Axial (top), coronal (middle) and sagittal (bottom) views of the segmented lung are represented with the respective mapped volume according to CNN classification: consolidation (C, cyan), fibrosis (F, orange), ground glass opacity (GGO, yellow), healthy (H, green), low attenuation areas (LAA, blue), reticulation (R, fuchsia). Patient 1 (FEV1 = 110%, FVC = 100%) shows a prevalence of N (green, 58%) and with relevant manifestation of GGO (yellow, 41%) in the lower lung and negligible presence of other cHP patterns (C, F, R, LAA < 1%). Patient 2 (FVC = 39%, FEV1= 33%) is characterized by extensive GGO all over lung parenchyma (yellow, 71%), moderate R (fuchsia, 21%) and a low extent of H (green, 5%). C, F and LAA were negligible (C, 1%; F, 1% and LAA 1%).

PReLU layers was aimed at minimizing fine tuning from the user as it allows adaptive learning of the parameters of the rectifiers without assigning deterministic values a priori without increasing the computational cost (33). On the test set, the confusion between reticular and fibrotic patterns is due to their common fibrotic nature and contributes a major share to the overall error as observed also by (13).

We applied the trained network to an independent cohort of 27 cHP patients. H, GGO, and R were the most extensive patterns, whereas LAA was negligible. Mosaic attenuation pattern, defined by the Fleischner society as lobular areas of decreased attenuation and vascularity (5), was previously reported with high frequency in cHP, suggesting small-airways involvement and air trapping (6,7). Our quantitative analysis shows that the extent of LAA in our population was minimal (less than 1% of the total parenchyma), even though mosaicism was present in 37% of patients. These results are in accordance with Jacob and colleagues (34), who also reported minimal air trapping in their cHP patients (<1% of the lung parenchyma), which gradually decreased with increasing disease severity. This supports the idea that visual CT assessment can mistakenly classify normal lung areas as LAA: regions with increased density may produce a low-density appearance in the adjacent normal lung parenchyma, thereby mimicking LAA. This is also supported by histological studies: despite significant bronchiolar involvement, histological cHP samples have not described alveolar overdistention in the residual, nonfibrotic lung parenchyma (35).

Correlations between CT features and PFTs were consistent with previous publications (36,37), showing that pulmonary functional indices are negatively correlated to the extent of CT features of fibrosis and that the reduction of DLCO is related to the extent of F and not to LAA. Our results are in contrast with Hansell et al. (6), who reported a relationship between the extension of LAA and the increased RV and RV/TLC indexes. However, in their study, they used a visual semiquantitative score and PFTs were not performed in all patients, compromising the extrapolation of the results in such a small sample.

Patients with mosaic attenuation pattern have a larger extent of normal lung parenchyma and significantly more preserved lung function than patients with nonmosaic attenuation. This suggests that in HP mosaic attenuation pattern can represent the patchy involvement of this disease, reflecting a

TABLE 4. Percentages of Lung Abnormalities According to Mosaic Attenuation Classes in Inspiration and Correlation with Lung Function Parameters

	Nonmosaic attenuation ($n = 17$)	Mosaic Attenuation ($n = 10$)	p
cHP Pattern Extension [%]			
C	**0.68 (0.36–1.24)**	**0.08 (0.00–0.41)**	**0.009**
F	1.01 (0.43–1.39)	0.350 (0.130 - 1.317)	0.14
GGO	62.82 ± 11.99	63.58 ±8.40	0.86
H	**20.75 ± 8.87**	**29.439 ± 12.360**	**0.04**
LAA	0.120 (0.035–0.745)	0.38 (0.08–1.13)	0.21
R	**12.10 (4.68–20.82)**	**3.30 (2.13–9.14)**	**0.02**
PFTs			
TLC (L)	3.33 ±1.00	3.41 ± 0.79	0.45
TLC (%)	61 ± 12.63	72 ± 20.99	0.22
RV (L)	1.15 (1.02–1.50)	1.26 (1.14–1.46)	0.47
RV (%)	70 (60.50–79.50)	87 (70.30–95.50)	0.14
RV/TLC	0.39 ± 0.06	0.40 ± 0.07	0.65
RV/TLC (%)	137 ± 3.20	154 ± 43.40	0.75
FVC (L)	1.96 ± 0.61	2.08 ± 0.72	0.82
FVC (%)	**52.90 ± 10.74**	**63.90 ± 22.90**	**0.04**
FEV1 (L)	1.48 (1.32–2.35)	1.80 (1.32–2.06)	0.71
FEV1 (%)	58 ± 11.41	68 ± 20.63	0.10
FEV1/FVC	0.88 ± 0.04	0.87 ± 0.06	0.61
FEV1/FVC (%)	106 (105–116)	109 (105–113)	0.98
FEF25-75 (L/s)	2.44 (2.21–3.22)	2.60 (1.95–3.18)	0.90
FEF25-75 (%)	95 ± 26.48	107.7 ± 35.57	0.27
DLCO	9.32 (6.74–16.24)	11.95 (9.23–17.64)	0.33
DLCO (%)	**35 (29–52)**	**49 (41–74)**	**0.05**

Abbreviations: C, consolidation; DLCO, pulmonary diffusion of carbon monoxide; F, fibrosis; FEV1, forced expiratory volume in one second; FEF25-75, forced mid-expiratory flow rate; FVC, forced expiratory capacity; GGO, ground glass opacities; H, healthy; LAA, low attenuation areas; R, reticulation; RV, residual volume; TLC, total lung capacity. Statistically significant relations are highlighted in bold.

Data are reported as mean ± standard deviation if normally distributed or median (25^{th}–75th percentile) otherwise.

.

continuum of lung impairment. In early stages such as in subacute (or nonfibrotic) HP, when bronchiolar involvement is preponderant, the mosaic attenuation pattern may represent small-airways involvement and air trapping, reflecting different time constants of filling and emptying of pulmonary lobules in more preserved lungs. Alternatively, in chronic/fibrotic HP, mosaic attenuation pattern could more likely represent less affected, normal lobular areas within ground-glass interstitial or airspace infiltration areas. Our findings reinforce that mosaic attenuation is not always synonymous with air trapping in cHP as suggested previously (7). Rather, we suggest that, contrary to subacute or nonfibrotic HP, cHP is mainly a restrictive disease. Of note, in this same population, we have performed forced oscillations exams and investigated inspiratory capacity in CPFE, finding no evidence of small airway involvement or dynamic hyperinflation during exercise, besides significant mosaicism on CT (38,39). Our results agree with (40), who found that evidence of mosaic attenuation in biopsy-proven cHP predicted better survival, even after adjusting for clinical characteristics and distribution of fibrosis. It remains unclear why patients with mosaic attenuation appear to exhibit different clinical courses. It is possible that patients with greater levels of mosaic attenuation may represent the initial stage of the disease, a different phenotype with more airway involvement compared to interstitial fibrosis, or simply greater responsiveness to immunosuppressive therapy or antigenic exposure cessation. Longitudinal studies are needed to understand the role of mosaic attenuation in disease progression.

Our study has some strengths, including inclusion of patients with a definite/high confidence HP diagnosis according to the most recent published guidelines (3). Although new diagnostic criteria were just recently published, at the time of study recruitment, we have used fibrosis detected on CT scans or histological samples as one of the criteria for "chronic HP," meaning our cohort does have patients now named "fibrotic HP." Also, "typical HP" with mosaic attenuation is represented in almost one-third of our cohort. Patients within the "indeterminate tomography" category were not included in our study. Additionally, at the time of the study recruitment, we also considered known antigenic exposure, compatible histology on transbronchial biopsies, and lymphocytosis on BAL as criteria for a confident HP diagnosis, since pprecipitins and bronchoprovocation tests are not available in our clinic. In conclusion, our patient cohort is composed of patients with either a "definite" or "high confidence" diagnosis of HP according to the most recent guidelines (3).

Our study has limitations. The number of patients was relatively low, due to the strict inclusion criteria of the broader study protocol. However, these strict criteria resulted in high homogeneity within the groups, leading to high statistical significance. Also, our cohort of patients included those with less severe disease since patients had to perform exercise testing as part of a broader protocol, this may limit generalizability to those with more severe disease. Furthermore, our patient cohort was composed of patients with a low smoking burden, to avoid confounding with small airway involvement and smoking. Finally, our cohort did not include patients with farmer's lung, in which the presence of emphysema is classically described (41). Further studies will require the inclusion of patients with other exposures and less severe disease. Finally, air trapping selections were underrepresented in the original public database and had to be grouped with emphysematous regions and classified as LAA. Additional air trapping regions with corresponding expiratory scans should ideally be added to the training set to allow ungrouping LAA into its constituent patterns.

Longitudinal follow up with prospective imaging and clinical data may help monitoring disease in clinical practice, predicting treatment responsiveness and outcomes.

As regard the methodological approach, no direct comparison to previous works is possible due to either the use of

different datasets or the consideration of different patterns. Although we did not consider regions presenting more than one pattern, accuracy is comparable with (13) despite a shallower network architecture. Future developments involve the inclusion of regions with mixed patterns as well as possible comorbidities.

In conclusion, our study presents a CNN method to detect and quantify cHP-associated textural patterns, with high correlation to PFTs. Besides significant mosaic attenuation, LAA in fibrotic disease can represent preserved normal areas in the middle of fibrosis and not necessarily air trapping. CNN analysis can improve cHP diagnosis and characterization, providing a tool for longitudinal studies.

FUNDING

OMD received a grant from the European Respiratory Society, Short-Term Research Fellowship 2015 for this project.

REFERENCES

1. Lacasse Y, Girard M, Cormier Y. Recent advances in hypersensitivity pneumonitis. Chest 2012; 142:208–217. doi:10.1378/chest.11-2479.
2. Vasakova M, Morell F, Walsh S, et al. Hypersensitivity pneumonitis: perspectives in diagnosis and management. Am J Respir Crit Care Med 2017; 196:680–689. doi:10.1164/rccm.201611-2201PP.
3. Raghu G, Remy-Jardin M, Ryerson CJ, et al. Diagnosis of hypersensitivity pneumonitis in adults. Off ATS/JRS/ALAT Clin Pract Guideline 2020. doi:10.1164/rccm.202005-2032ST.
4. Dias OM, Baldi BG, Pennati F, et al. Computed tomography in hypersensitivity pneumonitis: main findings, differential diagnosis and pitfalls. Expert Rev Respir Med 2018; 12:5–13. doi:10.1080/17476348.2018.1395282.
5. Hansell DM, Bankier AA, MacMahon H, et al. Fleischner society: glossary of terms for thoracic imaging. Radiology 2008; 246:697–722. doi:10.1148/radiol.2462070712.
6. Hansell DM, Wells AU, Padley SPG, et al. Hypersensitivity pneumonitis: correlation of individual CT patterns with functional abnormalities. Radiology 1996; 199:123–128. doi:10.1148/radiology.199.1.8633133.
7. Small JH, Flower CDR, Traill ZC, et al. Air-trapping in extrinsic allergic alveolitis on computed tomography. Brain Lang 1996; 51:684–688.
8. Uppaluri R, Hoffman EA, Sonka M, et al. Computer recognition of regional lung disease patterns. Am J Respir Crit Care Med 1999; 160:648–654. doi:10.1164/ajrccm.160.2.9804094.
9. Xu Y, van Beek EJR, Hwanjo Y, et al. Computer-aided classification of interstitial lung diseases via MDCT: 3D adaptive multiple feature method (3D AMFM). Acad Radiol 2006; 13:969–978. doi:10.1016/j.acra.2006.04.017.
10. Depeursinge A, Pad P, Chin AS, et al. Optimized steerable wavelets for texture analysis of lung tissue in 3-D CT: classification of usual interstitial pneumonia. Proc - Int Symp Biomed Imaging 2015: 403–406. doi:10.1109/ISBI.2015.7163897. 2015-Julyhttps://doi.org/.
11. Vo KT, Sowmya A. Multiscale sparse representation of high-resolution computed tomography (HRCT) lung images for diffuse lung disease classification. Proc - Int Conf Image Process ICIP 2011: 441–444. doi:10.1109/ICIP.2011.6116545.
12. Sluimer IC, Van Waes PF, Viergever MA, et al. Computer-aided diagnosis in high resolution CT of the lungs. Med Phys 2003; 30:3081–3090. doi:10.1118/1.1624771. https://doi.org/.
13. Anthimopoulos M, Christodoulidis S, Ebner L, et al. Lung pattern classification for interstitial lung diseases using a deep convolutional neural network. IEEE Trans Med Imaging 2016; 35:1207–1216. doi:10.1109/TMI.2016.2535865.
14. Walsh SLF, Calandriello L, Silva M, et al. Deep learning for classifying fibrotic lung disease on high-resolution computed tomography: a case-cohort study. Lancet Respir Med 2018; 6:837–845. doi:10.1016/S2213-2600(18)30286-8.
15. Gao M, Bagci U, Lu L, Wu A, et al. Holistic classification of CT attenuation patterns for interstitial lung diseases via deep convolutional neural networks. Comput Methods Biomech Biomed Eng Imaging Vis 2018; 6:1–6. doi:10.1080/21681163.2015.1124249.
16. Mets OM, Zanen P, Lammers JWJ, et al. Early identification of small airways disease on lung cancer screening CT: comparison of current air trapping measures. Lung 2012; 190:629–633. doi:10.1007/s00408-012-9422-8.
17. Wanger J, Clausen JL, Coates A, et al. Standardisation of the measurement of lung volumes. Eur Respir J 2005; 26:511–522. doi:10.1183/09031936.05.00035005.
18. MacIntyre N, Crapo RO, Viegi G, et al. Standardisation of the single-breath determination of carbon monoxide uptake in the lung. Eur Respir J 2005; 26:720–735. doi:10.1183/09031936.05.00034905.
19. Miller MR, Hankinson J, Brusasco V, et al. Standardisation of spirometry. Eur Respir J 2005; 26:319–338. doi:10.1183/09031936.05.00034805.
20. de CA, Pereira C, Sato T, et al. New reference values for forced spirometry in white adults in Brazil. J Bras Pneumol 2007; 33:397–406 http://www.scielo.br/scielo.php?script=sci_arttext&pid=S1806-37132007000400008&nrm=iso.
21. Neder JA, Andreoni S, Peres C, et al. Reference values for lung function tests. III. Carbon monoxide diffusing capacity (transfer factor). Brazilian J Med Biol Res 1999; 32:729–737. doi:10.1590/S0100-879X1999000600008.
22. Depeursinge A, Vargas A, Platon A, et al. Building a reference multimedia database for interstitial lung diseases. Comput Med Imaging Graph 2012; 36:227–238. doi:10.1016/j.compmedimag.2011.07.003.
23. Li Q, Cai W, Wang X, et al. Medical image classification with convolutional neural network. In: 2014 13th Int. Conf. Control Autom. Robot. Vision, ICARCV 2014, 2014; 2014. p. 844–848. doi:10.1109/ICARCV.2014.7064414..
24. D.P. Kingma, J. Ba, Adam: a method for stochastic optimization, (2014) 1−15. http://arxiv.org/abs/1412.6980.
25. Sun Y, Wong AKC, Kamel MS. Classification of imbalanced data: a review. Int J Pattern Recognit Artif Intell 2009; 23:687–719. doi:10.1142/S0218001409007326.
26. F. Chollet, Keras, (2015). https://keras.io
27. Abadi M, Barham P, Chen J, et al. TensorFlow: a system for large-scale machine learning. In: In: Proc. 12th USENIX Conf. Oper. Syst. Des. Implement. Berkeley, CA, USA. USENIX Association; 2016:265–283 http://dl.acm.org/citation.cfm?id=3026877.3026899.
28. Pennati F, Salito C, Aliverti A. Registration of lung CT images acquired in different respiratory ranges with 4DCT and HRCT. In: In: Proc. Annu. Int. Conf. IEEE Eng. Med. Biol. Soc. EMBS; 2015. p. 2936–2939. doi:10.1109/EMBC.2015.7319007.
29. Hu S, Hoffman EA, Reinhardt JM. Automatic lung segmentation for accurate quantitation of volumetric X-ray CT images. IEEE Trans Med Imaging 2001; 20:490–498. doi:10.1109/42.929615.
30. Frangi AF, Niessen WJ, Vincken KL, et al. Multiscale vessel enhancement filtering. In: Wells WM, Colchester A, Delp S, eds. Med. Image Comput. Comput. Interv. — MICCAI'98, Berlin Heidelberg, Berlin, Heidelberg: Springer; 1998:130–137.
31. Yoo RWTS, Ackerman MJ, Lorensen WE, et al. Engineering and algorithm design for an image processing API: a technical report on ITK - the insight toolkit. In: Westwood J, ed. Proc. of Medicine Meets Virtual Reality, IOS Press Amsterdam; 2002:586–592.
32. Silva CIS, Müller NL, Lynch DA, et al. Chronic hypersensitivity pneumonitis: differentiation from idiopathic pulmonary fibrosis and nonspecific interstitial pneumonia by using thin-section CT. Radiology 2008; 246:288–297. doi:10.1148/radiol.2453061881.
33. K. He, X. Zhang, S. Ren, et al, Delving deep into rectifiers: surpassing human-level performance on ImageNet classification, (2015). http://arxiv.org/abs/1502.01852 (accessed September 19, 2019).
34. Jacob J, Bartholmai BJ, Rajagopalan S, et al. Automated computer-based CT stratification as a predictor of outcome in hypersensitivity pneumonitis. Eur Radiol 2017; 27:3635–3646. doi:10.1007/s00330-016-4697-4.
35. Grunes D, Beasley MB. Hypersensitivity pneumonitis: a review and update of histologic findings. J Clin Pathol 2013; 66:888–895. doi:10.1136/jclinpath-2012-201337.
36. Wells AU, Desai SR, Rubens MB, et al. Composite physiologic index derived from disease extent observed by computed tomography. Am J Respir Crit Care Med 2003; 167:962–969. doi:10.1164/rccm.2111053.
37. Jacob J, Bartholmai BJ, Rajagopalan S, et al. Automated quantitative computed tomography versus visual computed tomography scoring in idiopathic pulmonary fibrosis validation against pulmonary function. J Thorac Imaging 2016; 31:304–311. doi:10.1097/RTI.0000000000000220.
38. Dias OM, Baldi BG, Ferreira JG, et al. Mechanisms of exercise limitation in patients with chronic hypersensitivity pneumonitis. ERJ Open Res 2018; 4:00043–02018. doi:10.1183/23120541.00043-2018.

39. Dias OM, Baldi BG, Chate RC, et al. Forced oscillation technique and small airway involvement in chronic hypersensitivity pneumonitis. Arch Bronconeumol 2019; 55:519–525. doi:10.1016/j.arbres.2019.01.022.
40. Chung JH, Zhan X, Cao M, et al. Presence of air trapping and mosaic attenuation on chest computed tomography predicts survival in chronic hypersensitivity pneumonitis. Ann Am Thorac Soc 2017; 14:1533–1538. doi:10.1513/AnnalsATS.201701-035OC.
41. Erkinjuntti-Pekkanen R, Rytkönen H, Kokkarinen JI, et al. Long-term risk of emphysema in patients with farmer's lung and matched control farmers. Am J Respir Crit Care Med 1998; 158:662–665. doi:10.1164/ajrccm.158.2.9710012.